ISSN: 2472-3703 DOI: 10.6911/WSRJ.202504_11(4).0010

Based on Convolutional Neural Network Study of CT Images of Ovarian Cystadenoma

Ruofeng Yu[1], Yating Wu[2], Ruoyu Yu[3], Shou Fang[4,*]

[1]School of Chinese-Western Medicine, Fujian University of Traditional Chinese Medicine Fuzhou Fujian, China

[2]School of Humanities and Management, Fujian University of Traditional Chinese Medicine Putian Fujian, China

[3]School of Law, Xiamen University Tan Kah Kee College Zhangzhou Fujian, China

[4]Radiographic Imaging Management, Affiliatd Hospital of Putian University Fuzhou Fujian, China

[*] Corresponding author: Shou Fang (Tel: 0086-594-13859896633)

Abstract

Cystadenoma of the ovary is a disease that occurs in the ovary. In order to realise automatic segmentation of ovarian CT images, an improved U-net model based lesion segmentation method of ovarian cystadenoma CT images was proposed. VGG16 was used as the encoder to further simplify the structure of U-net model, and combined with CT image features for data enhancement. An ovarian CT image dataset was constructed based on clinical diagnosis data, and the model was trained and evaluated. The model achieved an Intersection over Union (IoU) of 88.85% on the test set, and an Area Under the Curve (AUC) of 99.72%, indicating the feasibility and accuracy of the improved U-net model for the segmentation of ovarian cystadenoma lesions. In comparison with the original U-net model, the proposed method can reduce the size of the model without compromising the accuracy of segmentation, and is more suitable for auxiliary clinical diagnosis.

Keywords

Medical image segmentation, U-net, Deep learning, ovarian cystadenoma.

1. INTRODUCTION

Ovarian cystadenoma (OvarianCystadenoma) is a prevalent clinical tumour of ovarian epithelial tissue origin, which can be categorised into serous cystadenoma and mucinous cystadenoma according to pathological types [1].According to literature [2], the malignant transformation rate of mucinous cystadenoma is 5% to 10%, and that of serous cystadenoma is as high as 35%, emphasising the necessity for prompt surgical intervention. The prognosis of lesions with different biological behaviours varies greatly, and preoperative imaging evaluation is therefore of particular importance [3].The rapid development of medical imaging technology has greatly facilitated clinical diagnosis and treatment. CT imaging, in particular, due to its high sensitivity and clarity, has an accuracy rate of 92.59% in the diagnosis of ovarian cystadenoma, achieving a relatively ideal result [4].

In recent years, image segmentation models based on deep learning have been extensively utilised in the domain of medical image processing [5].In literature [6], the U-net model is proposed on the basis of the full convolutional neural network (FCN) [7] for medical image

ISSN: 2472-3703 DOI: 10.6911/WSRJ.202504_11(4).0010

segmentation. The U-net model utilises the symmetrical U-shaped structure of downsampling and upsampling to capture higher-order context information and accurate target positioning, respectively. The up-sampling stage employs a jump connection to combine lower-order features and recover target details.A significant challenge in medical image segmentation is the scarcity of training data. To address this, U-net employs elastic deformation to enhance the available training images, a crucial step in medical image segmentation given the prevalence of deformation in human tissues. This operation effectively simulates actual deformation, enhancing the model's robustness. The U-net structure is adept at utilising both low-order and high-order semantic features present in medical images. In comparison with other image segmentation models, the U-NET structure is less complex and has a smaller number of parameters, and the number of training samples required is significantly reduced, making it difficult to overfit. These characteristics make U-net an overwhelming advantage in medical image segmentation tasks.

The application of image segmentation technology based on deep learning is currently focused on supporting the diagnosis of superficial diseases, with research on deep organs and tissues in vivo being in its infancy. The accurate segmentation of organs, tumours, blood vessels and other tissues in medical images is fundamental for 3D visualisation of medical images, graphic-guided surgery, follow-up disease diagnosis and precise treatment. However, the research and application of deep learning image segmentation technology in the field of obstetrics and gynecology in China is still in its infancy, and the current research results have not been used to segment CT images of gynecological diseases such as ovarian cystadenoma. The main challenges are as follows: Firstly, the organs and tissues in ovarian CT images are complex and irregular in shape, which can easily cause aliases of similar areas. Secondly, the lesion area is divided into benign and malignant, and the difference between these two image features is too large, resulting in oscillations in the model learning process and difficult convergence. Furthermore, the CT imaging findings of cystadenoma of the ovary bear a strong resemblance to those of other ovarian tumour diseases, which results in a limited number of suitable training samples and consequently increases the difficulty of medical image data collection.

The present paper proposes a solution to the aforementioned problems in the form of an automatic segmentation of cystadenoma in ovarian CT images based on an improved U-net.The convolutional layer structure in VGG16 [8] was used to replace the contraction path and expansion path of the original U-net, and the number of original convolutional nuclei was adjusted to further simplify the model, with a view to meeting the requirements of rapid response for clinically assisted diagnosis. The investigation further explores the potential of data enhancement and feature adjustment of CT images to facilitate the utilisation of image features by the model. Additionally, an ovarian CT image dataset was constructed for the training and evaluation of the model. The experimental evaluation results demonstrate the model's capacity to successfully segment ovarian cystadenoma lesions.

2. IMPROVED U-NET MODEL

2.1. U-shaped structure

The U-net network, characterised by its U-shaped structure, employs downsampling to acquire low-order feature information, thereby establishing the foundation for pixel recognition and classification. The high-order feature information can be obtained through upsampling, which facilitates accurate positioning of segmentation. The model's architecture is capable of capturing edge-related information concerning the lesion, enabling segmentation that closely resembles human performance, despite the utilisation of a limited number of training images. The skip connection facilitates the integration of low-order and high-order feature channels,

ISSN: 2472-3703 DOI: 10.6911/WSRJ.202504_11(4).0010

thereby ensuring the restoration of information that may have been lost during the convolution process. This contributes to a more precise segmentation. It is noteworthy that the number of skip connections in the U-net network structure is equivalent to the number of downsamples. This results in a more comprehensive feature recovery compared to that achieved by the FCN.

The improved U-net model algorithm utilised in this paper is depicted in Figure 1. The model algorithm comprises a contraction path on the left and an expansion path on the right. The algorithm's input is a medical image with a dimensions of 512×512 pixels, and following processing by the shrink path and the expansion path, the output is the segmentation of the lesions with the corresponding size. The contraction path follows the convolutional structure design of the VGG16 network, shrinking the feature map fourfold. Two convolution operations are applied for each contraction, with a 3×3 convolution kernel size and the ReLU activation function [9].To ensure that the input size of the feature map matches that of the current convolutional layer, the missing edge pixels are filled with zeros during the convolution process. Subsequent to the convolution operation, a 2×2 pooling operation is applied for downsampling. With each contraction, the number of feature channels is doubled and the size of the feature map is doubled. The number of convolutional nuclei for each contraction is set to (32, 64, 128, 256, 512) to simplify the network structure. The extended path is employed to extend the feature graph fourfold, with the core operation being upsampling, i.e. deconvolution. In order to recover the image size, the deconvolution step is set to two, thereby reducing the feature channel by half while doubling the image size. Following each extension, the feature graph of the contraction process is spliced with the feature graph of the expansion process using the jump join. Subsequently, two convolution operations are applied, with a 3×3 convolution kernel and the ReLU activation function. It is noteworthy that each expansion possesses an equal number of convolution nuclei to the contraction. Following four extensions, a convolution operation is applied, with a 1×1 convolution kernel and the ReLU activation function. The purpose of this step is to map the feature maps of the 32 channels into corresponding classes to obtain the final segmentation. The entire network consists of 23 convolutional layers. In comparison with the original U-net configuration, the number of convolutional nuclei at each level in the original U-net contraction path is (64, 128, 256, 512, 1024), respectively. The improved U-net configuration exhibits a reduced number of convolutional nuclei, thereby significantly diminishing the model's parameters. This reduction in complexity renders the model less susceptible to overfitting. Conversely, the segmentation speed of the model is accelerated, a critical consideration for clinical applications requiring real-time processing. Subsequent experiments will be conducted to assess the performance disparity between the enhanced U-net and the conventional U-net. Secondly, it has been observed that the output of the original U-net does not match the size of the input image. Although the output can be restored to the same size as the input by methods such as scaling, this may affect the effect of model segmentation. The improved U-net can ensure that the output image and the input image are the same size, and can be coupled directly.

2.2. Loss function

In the context of neural network training, the loss function is frequently employed to quantify the model's performance. Typically, the loss function receives two inputs: the model-predicted value and the true label value. The loss function calculates the difference between these two values and employs backpropagation to iteratively update the model parameters. Following multiple rounds of training and learning, the loss function converges to a minimum value, at which point the model achieves optimal performance. This paper proposes the use of multiple loss functions to guide model learning, and conducts experiments to identify the optimal loss function for the task at hand.

ISSN: 2472-3703 DOI: 10.6911/WSRJ.202504_11(4).0010

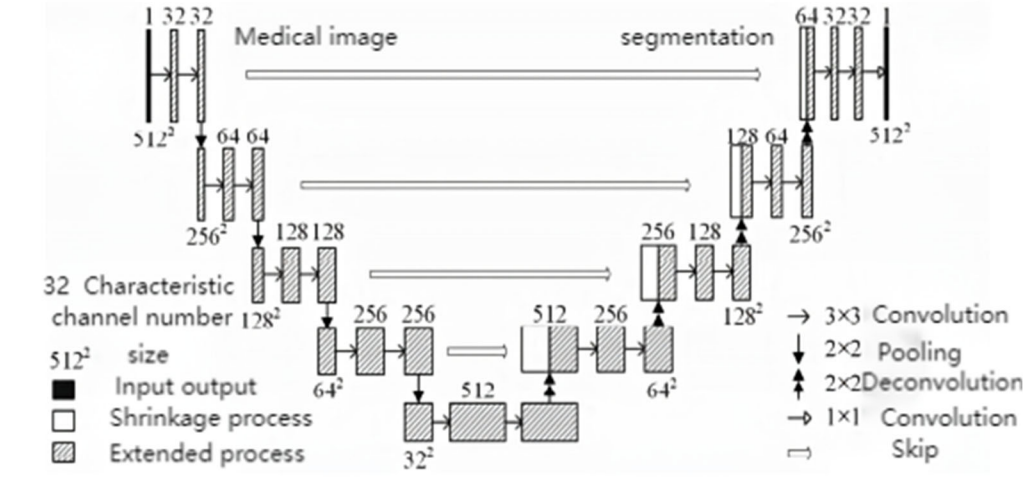

Figure 1. Improved U-net model algorithm flow

In image segmentation tasks, the loss function is typically based on two factors: pixel distribution and overlap degree (IoU). The BinaryCrossEntropy (BCE) loss function is a common example of the loss function based on pixel distribution, in which each pixel is examined separately and the category prediction is compared to the target vector (see equation 1).

$$BCE_{loss}(y,p) = -(y\log(p) + (1-y)\log(1-p)) \tag{1}$$

The formula (1) elucidates that the BCE_{loss} function treats all pixels equally. The label value y is represented as follows: $y = 1$ for positive examples and $y = 0$ for negative examples. The probability that the sample is a positive example is represented by p. However, when the number of target pixels is significantly smaller than the number of background pixels, the loss function can be seen to guide the model to learn how to better segment the background. This is contrary to the segmentation target and very unfriendly to medical images with extremely uneven targets and backgrounds. Therefore, this phenomenon can be alleviated by using WCE_{loss} function, as shown in equation (2). In this equation, β denotes the weight assigned to the positive sample, and it is typically set to a value greater than 1 during practical implementation.

$$WCE_{loss}(y,p) = -(\beta y\log(p) + (1-y)\log(1-p)) \tag{2}$$

The loss function, which is based on overlap degree, principally comprises the D_{ice} loss function. The D_{ice} loss function is derived from the D_{ice} coefficient, which is utilised to measure the similarity of two samples (see equation 3). Here, X represents the segmentation image predicted by the model, and Y represents the actual segmentation image. The $D_{ice\,loss}$ function is defined in equation 4, and it is applicable to cases where the samples are imbalanced.

$$D_{ice} = \frac{2|X\cap Y|}{|X|+|Y|} \tag{3}$$

$$D_{ice\,loss} = 1 - \frac{2|X\cap Y|}{|X|+|Y|} \tag{4}$$

ISSN: 2472-3703 DOI: 10.6911/WSRJ.202504_11(4).0010

Literature [10] enhanced the D_{ice} loss function and proposed the general D_{ice} loss function (G_{DL}), as demonstrated in equation (5). In this equation, r_{ln} denotes the real pixel category of class l in the n position, while P_{ln} represents the corresponding predicted probability value, and w_t signifies the weight of each class.

$$G_{DL} = 1 - 2\sum_{i=1}^{2} \frac{w_t \sum_n r_{ln} P_{ln}}{w_t \sum_n r_{ln} + P_{ln}} \tag{5}$$

Tversky Loss [11] is a generalized form of D_{ice} loss, as demonstrated in equation (6). X represents the segmented image predicted by the model, and Y represents the real segmented image. By adjusting the α and β parameters, the trade-off between the two can be controlled, and thus the segmentation results of the model can be influenced. For instance, when α and β are both 0.5, T_L degenerates into D_{ice} loss.

$$T_L = 1 - \frac{X \cap Y}{X \cap Y + \alpha|X - Y| + \beta|Y - X|} \tag{6}$$

3. DATA SETS

3.1. Data set construction

3.1.1 Data acquisition

To the best of the author's knowledge, no publicly available datasets on ovarian cystadenoma in the field of image segmentation are currently available. There are few studies on the segmentation of ovarian cystadenoma.In order to train and test the model, a new data set of ovarian CT images was constructed. The ovarian CT images used in this study were obtained from 12 patients with ovarian diseases, including serous papillary cystadenoma, mucinous cystadenoma, borderline cystadenoma and ovarian cancer, who were treated in the imaging Department of Putian University Affiliated Hospital in Fujian Province from 2019 to 2020. The CT images were sectioned with a thickness of 1.5 mm, and 10 to 80 CT images were obtained per case, depending on the lesion type.All cases underwent surgical resection of the lesion and were finally confirmed by postoperative pathological examination, ensuring the validity of the dataset.

A total of 12 patients' image data were screened, with images featuring complete lesion areas and clear edges selected for straightforward labelling. The initial and final CT images devoid of lesion areas were then removed from the CT image sequences.As illustrated in Figure 2, patient CT images frequently exhibit intrauterine interference, leading to aberrant CT values within the lesion area and subsequent oscillations during the model training process, thereby impeding model convergence. To address this issue, the present study opted for a manual cleansing of the dataset, a process that involved the elimination of such abnormal CT images.The final dataset comprised 985 valid images from 12 cases. The dataset used in this experiment was subsequently formed after the removal of sensitive information pertaining to the patient and the device.The training set comprised a total of 834 images from the first 10 cases, while the test set comprised a total of 151 images from the last two cases. U-net has been demonstrated to achieve near-human segmentation with very few training images; therefore, the amount of data used in this experiment is sufficient for training U-net.

ISSN: 2472-3703 DOI: 10.6911/WSRJ.202504_11(4).0010

Figure 2. The influence of IUD on CT images

3.1.2 Data annotation

Data annotation was conducted under the guidance and supervision of gynecologists and radiologists, with the physician determining the boundary of the lesion through the density, shape, and enhancement scanning enhancement mode, and further determining the labeling results in combination with intraoperative observation. The image annotation tool Labelme was employed for mask annotation, as illustrated in Figure 3. The annotated area completely covers the cystadenoma edge and fits the external contour as closely as possible to ensure the accuracy of segmentation. The label value is divided into two categories: the marked area is the focus, and the rest is the background. Once the annotation is complete, Labelme converts the result into a JSON file, which is then masked by a Python script to facilitate subsequent data processing.

Figure 3. Image labeling process

3.2. Data set construction

3.2.1 CT image processing

It is important to note the distinction between conventional images, which store the colour and grey value of pixels, and CT images, which store CT values in Hounsfield Units (H_U). The latter reflects the degree of X-ray absorption by human tissues.The medical image format adopted in this experiment is DICOM. In order to accurately reflect the object's true density, it is imperative to employ formula (7) to convert the original gray value stored in the DICOM file into the CT value. This process enables the extraction of the S_{lope} and $i_{ntercept}$ values from the DICOM metadata.

$$H_U = P_{ixel} \times S_{lope} + i_{ntercept} \quad (7)$$

ISSN: 2472-3703 DOI: 10.6911/WSRJ.202504_11(4).0010

The value range of CT values extends from [-1024, 3071], resulting in a low contrast of the image, which hinders the clarity of its features, thereby precluding the extraction of specific features for particular organs. In the field of medical imaging, window techniques are employed to select the range of CT values of interest. The Window Width (W_W) signifies the range of CT values displayed in a CT image, within which human tissue is presented in various analogue greyscales. Organisations exceeding this range are displayed in white, while those below this range are shown in black.No grey difference in the tissues exists beyond this range. Increasing the window width can extend the CT value range of the image display, allowing more tissues of varying densities to be displayed, thereby reducing the gray difference between tissues. Conversely, decreasing the window width can result in a smaller display range, and the gray difference between tissues will be increased. Window position (W_L), defined as the median of CT values displayed in CT images, is another factor to consider. The same window width will produce different viewing ranges due to different window positions. Once the window width and window position have been determined, the formula (8) can be utilised to calculate the upper and lower bounds of the CT image in terms of grey scale. Figure 4 demonstrates the effects of different window widths on the grey scale of CT images.

$$g_{rey\ level_{lower}} = W_L - \frac{W_W}{2}$$
$$g_{rey\ level_{upper}} = W_L - \frac{W_W}{2} \tag{8}$$

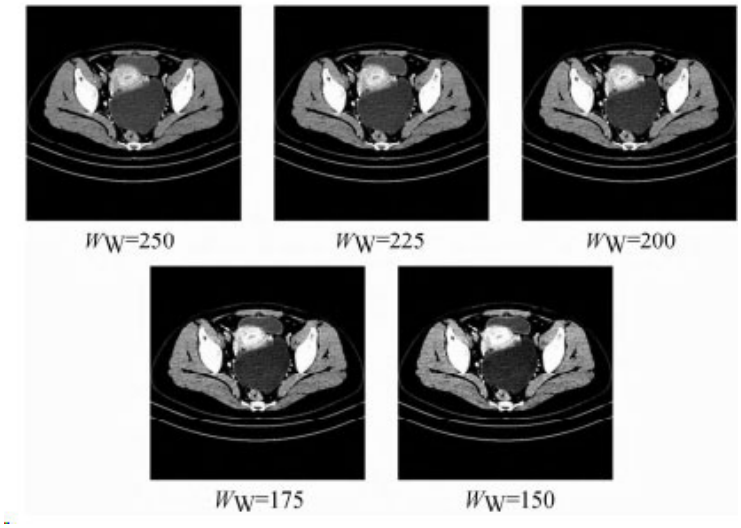

Figure 4. Image labeling process

In this paper, the experiment of window width is conducted in a distinct manner, and the window width parameter that yields the optimal segmentation effect is selected for subsequent experimentation. Moreover, the pixel value in the screen that exceeds the specified range is set to 0, thereby preventing other irrelevant pixels from impacting the segmentation process.

3.2.2 Data enhancement

In conventional neural network tasks, the most effective approach to prevent model overfitting and enhance model generalisation capability is to augment the size of the data set. However, acquiring substantial medical image data sets is challenging due to the necessity of expert annotation, which is time-consuming and labour-intensive. Consequently, data enhancement techniques are frequently employed during practical model training to expand existing data sets.

ISSN: 2472-3703 DOI: 10.6911/WSRJ.202504_11(4).0010

Data enhancement is the process of utilising image processing techniques to expand the capacity of limited data sets to produce similar outcomes to those of larger data sets without increasing the volume of original experimental data. A third-party image processing library is employed to implement geometric transformations on the original image, encompassing operations such as rotation, deformation, scaling, and distortion. During the enhancement process, the fundamental feature information of the image, including the grey-level and texture characteristics of the lesion, remains constant. The enhanced image is depicted in Figure 5. It is imperative to acknowledge that data enhancement is exclusively executed during the model training phase. Subsequent to data enhancement, the number of training sets was augmented from 834 to 1406, thereby enabling the successful training of the model.

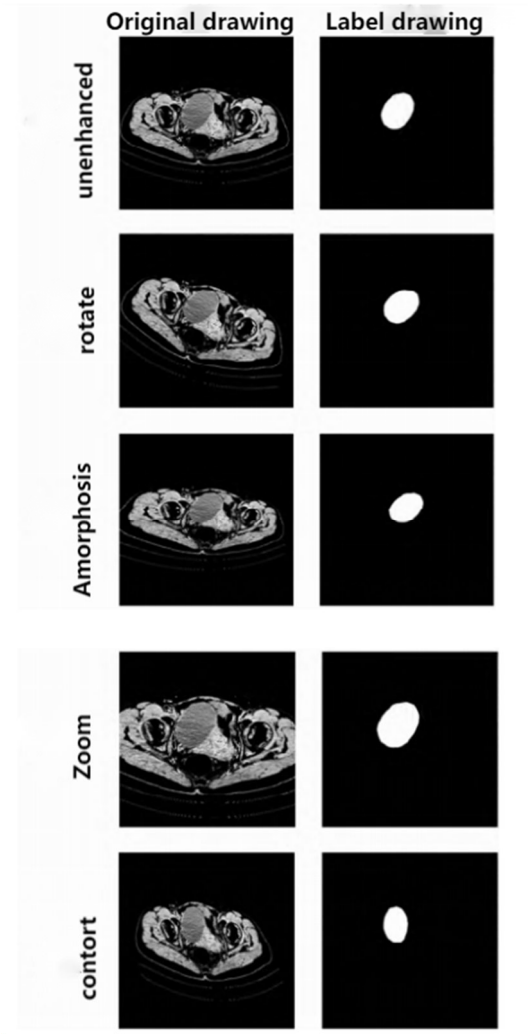

Figure 5. Data enhanced image and its label

4. ACTUAL TEST

4.1. Evaluation index

In this paper, the following indexes were utilised to assess the performance of the ovarian cystadenoma segmentation model. Concurrently, the actual segmentation effect was observed to comprehensively evaluate the segmentation ability of the model.

4.1.1 Dice

The dice coefficient is a metric employed for the evaluation of a segmentation model's capability in delineating the similarity between two samples. The value range is [0,1]. It is

ISSN: 2472-3703 DOI: 10.6911/WSRJ.202504_11(4).0010

widely accepted that a higher value indicates a better model performance. As demonstrated in equation (9), where T_P, F_P and F_N denote true, false positive and false negative cases, respectively.

$$D_{ice} = \frac{2T_P}{2T_P+F_N+F_P} \tag{9}$$

4.1.2 AUC

The Area Under the Curve (AUC) index is a metric that quantifies the area under the Receiver Operating Characteristic (ROC) curve. This index is frequently employed to assess the efficacy of binary classifiers.

4.1.3 Accuracy

Accuracy is a frequently employed metric for evaluating the segmentation capability of a model. This is measured by the ratio of pixels that have been correctly categorised to the total number of pixels, as depicted in equation (10)

$$A_{ce} = \frac{T_P+T_N}{T_P+T_N+F_N+F_P} \tag{10}$$

4.1.4 Precision

The accuracy rate is defined as the proportion of samples that are positive among the samples predicted by the model. The closer to 1, the better, as demonstrated in equation (11).

$$P_{recision} = \frac{T_P}{T_P+F_P} \tag{11}$$

4.1.5 Recall

The recall rate, also known as the precision rate, is defined as the proportion of samples predicted by the model to be positive that are in fact positive, with a value as close to 1 as possible, as illustrated in equation (12).

$$R_{ecall} = \frac{T_P}{T_P+F_N} \tag{12}$$

4.2. Experimental results and model evaluation

The present paper comprises three sets of experiments. Firstly, the effects of different window widths on model learning are compared. Then, the use of different loss functions to learn the model is investigated, and the experimental results are analysed. Finally, the improved U-net model is compared with the original U-net model to verify the effect of the improved model on the segmentation results. Finally, the optimal parameters identified in the preceding experiments are utilised for the definitive segmentation of the lesions, and the resulting segmentation outcomes are evaluated based on the authentic lesions labelled images. The hyperparameters employed in the experimental setup are enumerated in Table 1.

ISSN: 2472-3703 DOI: 10.6911/WSRJ.202504_11(4).0010

Table 1. Hyperparameter setting

Hyperparameter	Value
Batch size	4
Window center	-896
Learning rate	0.00001
Loss function	Dice Loss
Epoch	50

4.2.1 The influence of different window width values

The width of the window has been demonstrated to have an effect on the contrast of CT images. In order to explore the influence of different window widths on model learning, this paper adjusted the window widths on the basis of the original window widths, and set the window widths to {150, 175, 200, 225, 250} respectively. Five independent experiments were conducted, and each experiment was repeated five times to obtain average results.

The experimental results are presented in Table 2. It can be observed that when the window width value is set to 175, the indicators of the segmentation result reach an optimal level. However, when the window width is less than 175 or greater than 175, the contrast of the CT images is excessively high or low, respectively, resulting in the loss of image features and suboptimal segmentation outcomes. In the subsequent experiment, 175 was utilised as the window width value.

Table 2. Index of segmentation results under different window width values

WW	Dice	Accuracy	AUC	Precisio	Recall
250	0.8598	0.9943	0.9393	0.8939	0.8255
225	0.8619	0.9943	0.9437	0.8979	0.8425
200	0.8723	0.9947	0.9492	0.9052	0.8514
175	0.8773	0.9950	0.9597	0.9091	0.8616
150	0.8758	0.9948	0.9535	0.8898	0.8754

4.2.2 The influence of different loss functions

In the domain of image segmentation, the selection of loss function has been shown to exert a significant influence on the training process of the model, resulting in divergent segmentation outcomes (see Table 3 for details). The present experiment involved the implementation of multiple loss functions, as outlined above, in a series of independent experiments. The objective of this approach was to investigate the impact of these functions on the segmentation of ovarian cystadenoma. In instances where WCE is employed, the parameter β is set to 2. For T_L, the values of α and β are set to 0.7 and 0.3, respectively. The ensuing experimental findings are delineated in Table 3.

Table 3. Index for dividing results under different loss functions

Loss	Dice	Accuracy	AUC	Precisio	Recall
GDL	0.8656	0.9945	0.9477	0.8986	0.8492
DL	0.8696	0.9948	0.9460	0.9087	0.8500
TL	0.8672	0.9940	0.9710	0.8304	0.9181
BCE	0.8761	0.9949	0.9943	0.8901	0.8781
WCE	0.8885	0.9951	0.9972	0.8626	0.9252

ISSN: 2472-3703 DOI: 10.6911/WSRJ.202504_11(4).0010

It is evident that the Dice coefficient and segmentation accuracy achieved by employing WCE are both optimal.In comparison with BCE, WCE allocates distinct weight factors to each category, thereby effectively addressing the issue of imbalanced sample categories, thus ensuring the optimal outcome in the distribution-based loss function. The loss function based on overlap degree employs a similar approach, utilising weighting to assign distinct weight parameters to false positive and false negative cases. This enables the regulation of the recall rate and accuracy rate of the model, thereby ensuring optimal performance of the loss function.It is noteworthy that GDL is designed for multi-classification tasks and is not fully equipped to leverage its full potential in binary classification segmentation tasks. Consequently, the segmentation effect is not as effective as that achieved by conventional DL.

Furthermore, the findings obtained by distribution-based loss functions (BCE, WCE) are typically superior to those obtained by loss functions based on overlap (DL, GDL, TL).To analyse the causes of this phenomenon, BCE and DL are used as exemplars. $\hat{y}$ is employed to represent the predicted value of the model, y is used to represent the label value of the real lesion, and the gradient of BCE and DL with respect to $\hat{y}$ is shown in equation (13). It is evident that when the predicted or true value is minimal, the gradient value of DL may be substantial, leading to oscillatory behaviour during backpropagation learning and consequent instability in the training process.

$$\nabla B_{CE} = \hat{y} - y$$
$$\nabla D_L = \frac{2y(y^2 - \hat{y}^2)}{(y^2 + \hat{y}^2)^2} \tag{13}$$

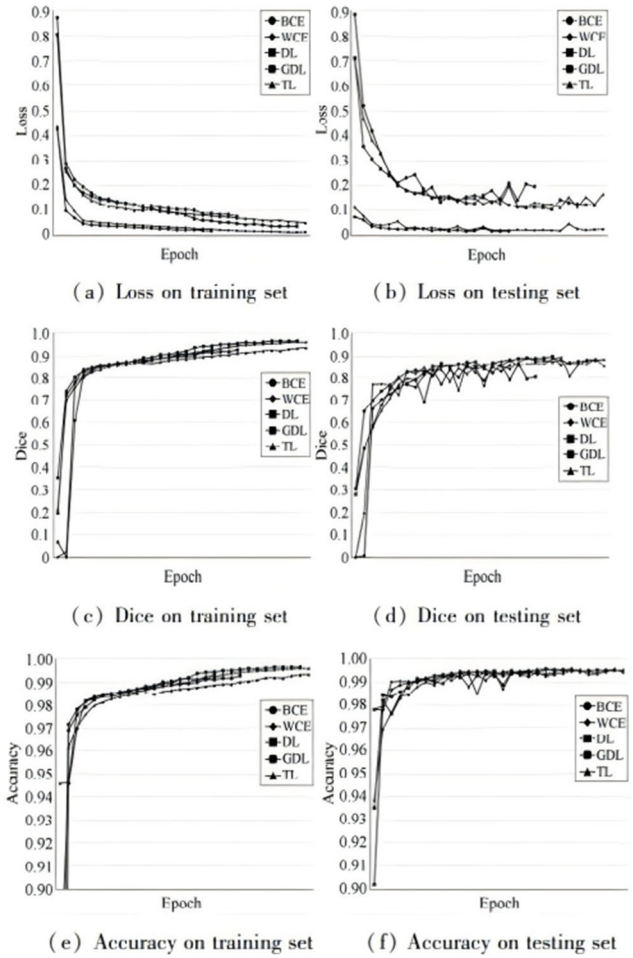

Figure 6. Metrics on the training set and test set

ISSN: 2472-3703 DOI: 10.6911/WSRJ.202504_11(4).0010

As illustrated in Figure 6, the learning process of the model is accompanied by alterations in various indicators. Utilising WCE during model learning results in optimal segmentation outcomes. Furthermore, an examination of the changes in each index curve on the test set reveals that the loss function based on overlap degree leads to oscillations in the model learning process. Consequently, its direct application as a loss function for guiding model training is not recommended.

4.2.3 Model improvement effect analysis

In this paper, we have refined the original U-net model to enhance its capacity for ovarian cystadenoma lesion segmentation. In order to verify the effect of the model improvement, a comparative experiment was conducted under the condition of a window width of 175 using the DiceLoss loss function. The effects that were observed both before and after the enhancement to the model are displayed in Table 4.

Table 4. Comparison of model improvement effect

Model	Dice	Accuracy	AUC	Precisio	Recall
Primitive	0.8674	0.9948	0.9329	0.9366	0.8231
Research	0.8696	0.9948	0.9460	0.9087	0.8500

It is evident that the enhanced model exhibits clear advantages over the original model with respect to the indicators. Concurrently, the enhanced model possesses a more streamlined network architecture, a reduced number of parameters, and a training process that is less susceptible to overfitting. Moreover, the simplified network configuration facilitates the model's capacity to fulfil the real-time performance demands of lesion segmentation during the testing phase.

4.2.4 Segmentation result analysis

In order to obtain the final segmentation result, the experimental parameter that yields the optimal outcome is selected, and the model obtained by the parameter is tested. The actual segmentation effect is demonstrated in Figure 7.

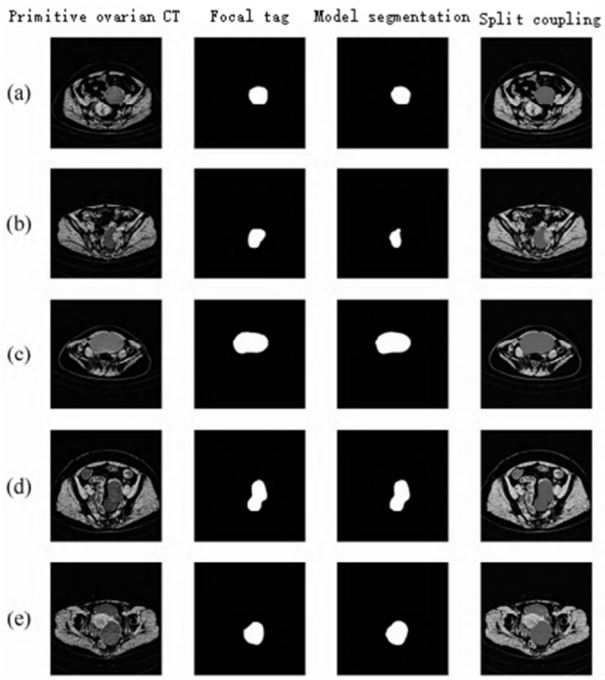

Figure 7. Model segmentation result

ISSN: 2472-3703 DOI: 10.6911/WSRJ.202504_11(4).0010

A comparison of the segmentation results of the model demonstrates that, in cases where the texture of the lesion area is regular, the model is able to achieve more accurate segmentation and coverage of the entire lesion area. As illustrated in Figure 7(b), the texture of the lesion area was found to be non-uniform. In the postoperative pathological diagnosis, the darker coloured area was identified as cystadenoma of the ovary, while the lighter coloured area exhibited signs of infiltration by cancer cells and was diagnosed as ovarian cancer. The model successfully segmented the focal region of cystadenoma of the ovary. However, due to the limited number of ovarian cancer cases in the training data set, the model did not adequately segment ovarian cancer. The experimental results demonstrate that the segmentation results produced by the enhanced U-net model using WCE as a loss function achieved an accuracy of 88.85%, signifying the efficacy of the enhanced U-net in attaining high accuracy. The clinical use standard is met by the segmentation results of the improved Unet.

The model requires 12 seconds to complete the segmentation of the entire test set, with an average processing time of 0.079 seconds per image. In the context of clinical diagnosis, the segmentation speed of the model is shown to be an effective tool for assisting physicians in identifying and segmenting focal areas. This finding underscores the viability and practical benefits of the model.

5. CONCLUSION

In order to achieve focal segmentation of cystadenoma of the ovary, CT images, an enhanced U-net network structure is proposed. VGG16 is utilised to substitute for the encoder in the original U-net, thereby simplifying the model structure. In this paper, clinical ovarian CT images are categorised and constructed into data sets. In order to address the paucity of data sets, data enhancement technology is employed to expand CT images. The efficacy of the model was evaluated using established metrics, and the results demonstrated the model's capacity for accurate segmentation, clear segmentation boundaries, and fulfilment of the criteria for clinical diagnostic and therapeutic use. The subsequent phase will entail the refinement of the model on the foundation of these accomplishments, with the objective of enabling the model to concurrently recognise a range of ovarian tumour diseases, including ovarian cystadenoma, endometriosis cyst, teratoma, and ovarian cancer, while achieving precise segmentation.

REFERENCES

[1] Liu Tingting, Qian Yong, Wang Xuemei, et al. The clinical value of CT and MRI in the diagnosis of ovarian cystadenoma [J]. Current Medicine, 2019,26(30):74-75. (in Chinese

[2] Qiang Jinwei, Zhou Kangrong, Liao Zhihe, et al. CT diagnosis of cystadenoma of ovary [J]. Journal of Practical Radiology,2004,20(3):253-256. (in Chinese)

[3] Wu Guoliang, Wang Shuping, Fu Guangyin, et al. Diagnostic value of CT and MRI for cystadenoma of ovary [J]. Chinese Research on Maternal and Child Health,2017,28(7):893-896.

[4] Sun L Z. Clinical analysis of CT and MRI diagnosis of cystadenoma of ovary [J]. Imaging Research and Medical Applications, 21,5(3):135-136.

[5] Chen Yidong, Zhang Qin, LAN LAN, et al. Application of deep convolutional neural networks in medical image segmentation [J]. Chinese Journal of Health Information Management,202118(2): 278-284.

[6] Ronneberger O,Fischer P, Brox T. U-Net: Convolutionalnetworks for biomedical image segmentation [C]//International Conference on Medical lmage Computing and Computer-Assisted Intervention ,2015 :234 -241.

ISSN: 2472-3703 DOI: 10.6911/WSRJ.202504_11(4).0010

[7] Long J, Shelhamer E, Darrell T. Fully convolutional net-works for semantic segmentation[J]. IEEE Transactions on Pattern Analysis and Machine Intelligence ,2015,39(4):640-651.

[8] Simonyan K, Zisserman A. Very deep convolutional net-works for large-scale image recognition[EB]. arXiv: 14091556v1 ,2014.

[9] Glorot X, Bordes A, Bengio YS. Deep sparse rectifier neu-ral networks [J]. Journal of Machine Learning Research, 2011.15 :315 -323.

[10] Crum W R,Camara O, Hill DLG. Generalized overlapmeasures for evaluation and validation in sMedical image a-nalysis[J]. EEE Transactions on Medical Imaging, 2006,25 :1451 -1461

[11] Salehi S, Erdogmus D, Gholipour A. Tversky loss function[19]for image segmentation using 3D fully convolutional deep net-works[C]//International Workshop on Machine Learning in Medical lmaging,2017:379 -387r